Dynamic polarization potential due to ^{6}Li breakup on ^{12}C

D. Y. Pang*
School of Physics and Nuclear Energy Engineering, Beihang University, Beijing 100191, China

R. S. Mackintosh†
Department of Physical Sciences, The Open University, Milton Keynes, MK7 6AA, United Kingdom
(Received 28 September 2011; published 19 December 2011)

For ^{6}Li scattering from ^{12}C at five laboratory energies from 90 to 318 MeV, we study the dynamic polarization potential, DPP, due to the breakup of the projectile. The breakup is evaluated using standard continuum discretized coupled-channels formalism applied to a two-body cluster model of the projectile. The DPP is evaluated over a wide radial range using both direct S-matrix-to-potential inversion and trivially equivalent local potential methods which yield substantially and systematically different results. The radius at which the real DPP changes from external repulsion to interior attraction varies systematically with energy. This should be experimentally testable because, according to notch tests, this crossover radius is within a radial range to which elastic scattering should be sensitive. The imaginary DPP has an emissive (generative) region at the lower energies; this may be associated with counterintuitive properties of $|S_L|$.

DOI: 10.1103/PhysRevC.84.064611 PACS number(s): 25.60.Gc, 24.50.+g, 24.10.Ht, 24.10.Eq

I. INTRODUCTION

We reopen an old question relating to the interaction potential between pairs of nuclei and the contribution to this potential that is made by excitations of the interacting nuclei. Such excitations contribute to the nucleus-nucleus interaction in ways that are not naturally described by models in which the local density assumption is implicit. Indeed, full understanding of the origin of specific features of the dynamic polarization potential (DPP) resulting from such excitations is still lacking; this seems a rather basic gap in our understanding of nuclear interactions. For example, just why does the specific process to be discussed here result in a repulsive term in the nuclear surface but an attractive term at smaller radii, and why (at certain energies) does the imaginary part of the DPP exhibit generative (emissive) radial regions?

It was found some 30 years ago that the real M3Y folding model potential required [1,2] a factor of about 0.6 in order to fit ^{6}Li elastic-scattering angular distributions (ADs). The explanation was found to lie in the breakup of the projectile, and a good representation of the scattering was found when the breakup was included using the continuum discretized coupled-channels (CDCC) formalism [3–7]. Exact inversion of the elastic-scattering S-matrix from such calculations [8] revealed explicitly the surface repulsion induced by the breakup of the projectile, and approximate inversion procedures revealed this too [5,6]; one of the themes of this paper is to draw out differences between the results of alternative inversion procedures. Later, S-matrix inversion revealed generic features of the DPP [9,10], arising from the breakup of deuterons as well as ^{6}Li, that were not confined to the nuclear surface: breakup consistently generates repulsion in the nuclear surface and attraction at smaller radii, with a marked oscillatory pattern in the nuclear interior. There is also further counterintuitive behavior discussed below.

In this work we study the DPP generated by the breakup of ^{6}Li scattering from ^{12}C at laboratory energies of 90, 123.5, 168.6, 210, and 318 MeV. In all calculations, a two-body cluster model of ^{6}Li is used and no excitations of ^{12}C are considered. Modest renormalization of the deuteron-^{12}C and ^{4}He-^{12}C interactions yields good fits to experimental ^{6}Li ADs when breakup coupling is included. Many features of the general approach followed here could be carried over to more recent extensions of the CDCC formalism, for example, Refs. [11–16].

Particular features of the work we describe are the following.

(i) A comparison is made between potentials derived from S-matrix inversion and the trivially equivalent local potential TELP algorithm. The differences at all energies are not small. Apart from the consequences for nuclear scattering dynamics, this also raises general questions about potential scattering. The real and imaginary volume integrals J_{R} and J_{IM}, as defined by Satchler [17], are well determined by inversion, providing a concise measure of the DPP.

(ii) The DPPs that we present are not confined to the surface region, and their overall properties, which we find to be well-established by inversion, vary in a consistent and systematic way with energy. Certain properties of the DPP can be linked to the fact that, at the lower end of the energy range studied, breakup coupling actually *increases* $|S_L|$ over a range of L.

(iii) The sensitivity of elastic scattering to the potentials within the nuclear overlap region is explored by means of notch tests. In principle, elastic-scattering ADs should be sensitive to the potential where the DPP changes from repulsive to attractive.

*dypang@buaa.edu.cn
†r.mackintosh@open.ac.uk

The potentials that we present are local and L-independent representations of underlying nonlocal and L-dependent potentials. As such, the behavior that we present has implications for rather basic properties of nucleus-nucleus potentials that cannot fully be accounted for within models based on the local density approximation.

Section II specifies the details of the CDCC calculations and the fits to the elastic scattering data. Section III explains and compares the methods leading to the DPPs and presents and compares the inverted potentials and the DPPs that are found. Section IV presents the notch tests that establish the radial sensitivity of the DPPs. Section V summarizes the results and suggests further work.

II. CDCC CALCULATIONS

Angular distributions for ^{6}Li scattering elastically from ^{12}C at 90, 123.5, 168.6, 210, and 318 MeV were reported in Refs. [18–21]. The experimental data for 90 MeV were obtained from the nuclear database EXFOR/CSISRS [22], and those for the other energies were obtained by digitizing from Refs. [19–21].

A standard three-body CDCC model was used in our analysis, based on an $\alpha + d$ cluster model of ^{6}Li in which the deuteron spin was omitted and the ground state was purely S wave. The $\alpha + d$ binding potential was taken to be of Woods-Saxon form with parameters $R = 1.9$ fm and $a_0 = 0.65$ fm [23–25]. The depth, 77.5 MeV, was adjusted to give the correct binding energy of ^{6}Li and was fixed for the calculation of the continuum states. Partial waves up to $L_{\max} = 1000$ were solved for the CDCC equations with projectile-target separations out to 1000 fm. Both Coulomb and nuclear breakup were included. The continuum bins were calculated with cluster separations $r \leqslant 50$ fm and the relative orbital angular momenta between α and d were included up to $l = 2$, higher l values having a small effect. The bin states were constructed by discretizing continuum states up to maximum $\alpha - d$ relative energies $\varepsilon_{\max} = 35.3$ MeV. The continuum states were divided into 15 bins, which are equally spaced in k space from $k = 0$ up to $k_{\max} = 1.5$ fm^{-1} with steps of 0.1 fm^{-1}. The coupling potentials were constructed with multipoles $q \leqslant 4$. The CDCC calculations were performed with FRESCO [26] and convergence in all cases was verified by calculations with an increased model space.

The real and imaginary parts of the $\alpha + {}^{12}$C and $d + {}^{12}$C potentials were obtained as follows: The starting point was the pair of potentials interpolated from the energy dependence of free α and d potentials [27], which were obtained by fitting $\alpha + {}^{12}$C and $d + {}^{12}$C elastic-scattering data from 10 to 100 MeV/nucleon using a single-folding model approach with the JLMB model nucleon-nucleus potentials Ref. [28], as described in Ref. [29]. The most appropriate context in which to isolate and study the contribution of breakup to the ^{6}Li optical potential is that in which the elastic-scattering AD is fitted. Accordingly, and unlike many CDCC calculations, the ^{6}Li ADs were fitted by normalizing the $d + {}^{12}$C and $\alpha + {}^{12}$C real and imaginary potentials with the same factors, $N_{\rm R}$ and $N_{\rm IM}$, for the real and imaginary parts, respectively. These

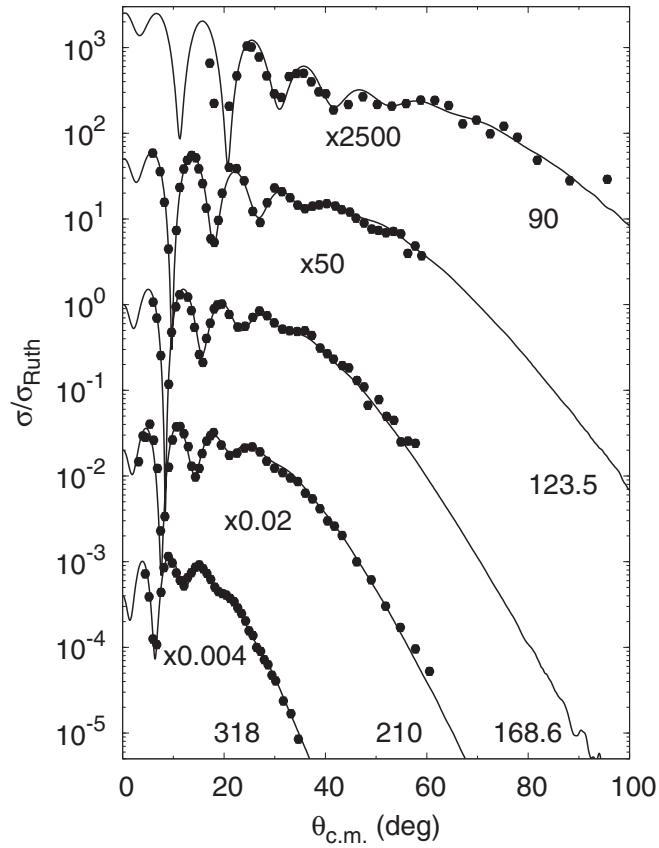

FIG. 1. Three-body CDCC calculations of ^{6}Li elastic scattering from ^{12}C at incident energies between 90 and 318 MeV. The dots are larger than the uniform error of 10% which was assumed for all data points. The measured and calculated cross sections are offset by a factor of 50 for clarity.

factors were therefore the normalization factors for the ^{6}Li-^{12}C folded potential that would be responsible for scattering if the breakup coupling were switched off. This folded potential is the 'bare" potential referred to in Sec. III below. The experimental ADs were fitted by searching upon $N_{\rm R}$ and $N_{\rm IM}$ assuming uniform uncertainties of 10% for all data points. Because automatic searching with a converged CDCC calculation is prohibitively time-consuming, the data were fitted by means of a grid search. The fits to the AD data are depicted in Fig. 1. The normalization factors $N_{\rm R}$ and $N_{\rm IM}$, for each energy, are listed in Table I. The DPPs themselves do not depend greatly upon changes in the optical potentials that are represented by

TABLE I. Real and imaginary renormalization factors $N_{\rm R}$ and $N_{\rm IM}$ for the $\alpha - {}^{12}$C and $d - {}^{12}$C potentials. The last two columns give volume integrals of the real and imaginary components in MeV fm^3.

$E_{\rm lab}$	$N_{\rm R}$	$N_{\rm IM}$	$J_{\rm R}$	$J_{\rm IM}$
90.0	0.85	1.15	326.34	141.52
123.5	0.85	1.15	314.24	139.45
168.6	0.85	1.10	298.95	138.00
210.0	0.90	1.05	302.82	133.40
318.0	0.90	1.05	272.16	136.15

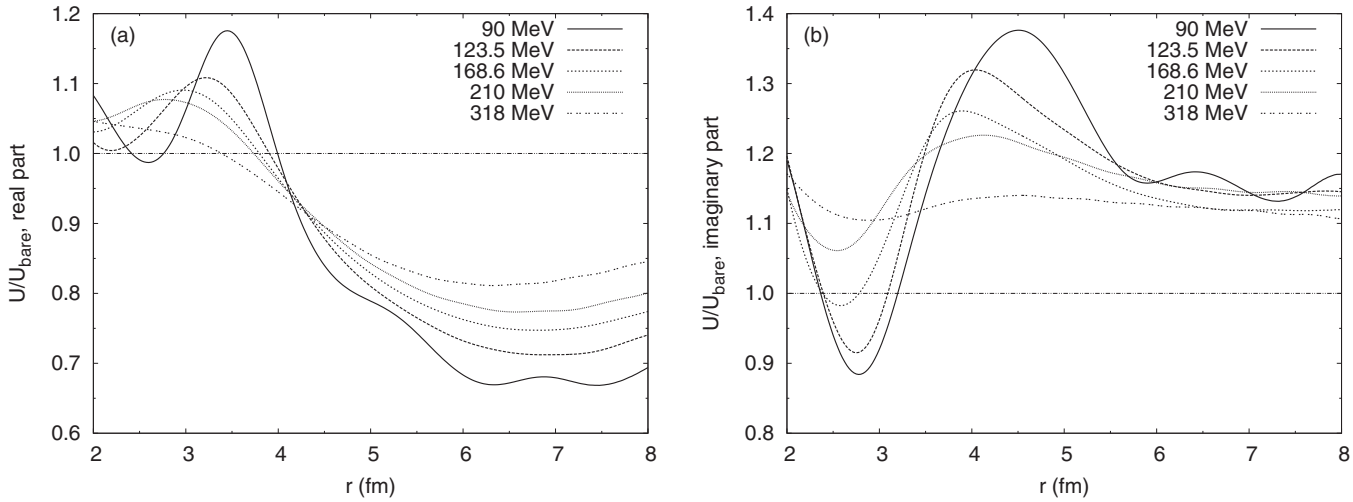

FIG. 2. Ratios between the full (bare + DPP) and the bare potentials for all five energies. Part (a) shows the ratio for the real part and part (b) shows the ratio for the imaginary part.

these normalization factors. Table I also includes the volume integrals J_R and J_{IM} of the real and imaginary components of the (normalized) bare potentials. The volume integrals are calculated following standard prescription [17], which includes the factor $(A_1A_2)^{-1}$ and the sign convention that J is positive for an attractive potential. Because only breakup processes are included explicitly in this work, all other reaction processes are represented through N_R and N_{IM}.

III. CALCULATION OF THE DPP

The formal DPP (see, e.g., Refs. [17,30]) is both nonlocal and L dependent. Nevertheless, almost all phenomenological or theoretical nucleus-nucleus potentials are local and L independent, often involving some local equivalent representation of exchange or other nonlocality. It is therefore natural to calculate local and L-independent equivalents to the underlying DPP, and that is reported here.

Calculation of the local equivalent of the formal DPP arising from the complete set of nonelastic processes is seldom attempted (but see, for example, Refs. [31,32] and references therein.) However, there have been many studies of DPPs due to specific coupled channels, early attempts include Refs. [33–36]. In the present work we determine the DPP that arises from one specific process, projectile breakup, by calculating the potential that exactly reproduces the S matrix, S_L, when that process is included in a reaction calculation, here a CDCC calculation. Subtracting the bare interaction from such a potential directly yields the DPP arising from the specific channels. Reference [37] gives an extensive discussion of this coupled-channels-plus-inversion procedure and its applications.

The local, L-independent potential that fits the S matrix is appropriate to making a connection between the local potential of standard phenomenology and the processes that fall outside local density models of the optical potential. Alternatives to S-matrix inversion exist, for example, Ref. [38]; some are compared in Ref. [39]; and Hussein *et al.* [40] discuss the relevance of different types of inversion to different situations. One such alternative to S-matrix inversion is the TELP [38], which, with appropriate partial wave weighting [41], can be output by the CC/CDCC code FRESCO [26]. A TELP potential is sometimes presented as the DPP due to specific processes. We shall directly compare the DPP calculated from the FRESCO TELP with the DPP calculated by S-matrix inversion.

Various techniques for S-matrix-to-potential inversion are surveyed in Ref. [42]; the results presented here exploit the iterative-perturbative (IP) procedure [8,42,43] that can yield precise inversions over a wide range of situations. This method is the basis of the code IMAGO [44], which can invert the S-matrix for spin-0, spin-$\frac{1}{2}$ and spin-1 projectiles.

TABLE II. For ^{6}Li scattering from ^{12}C at five laboratory energies, volume integrals ΔJ (in MeV fm^3) of the two components of the DPP induced by breakup of the projectile. The third column gives the change of rms radius of the real central component. The fourth column gives the change in total reaction cross section and the fifth column gives the breakup cross section.

E_{lab} (MeV)	ΔJ_R (MeV fm^3)	ΔR_{rms} (fm)	ΔJ_{IM} (MeV fm^3)	Δ CS (mb)	BU CS (mb)
90	−8.86	− 0.223	24.17	25.9	75.4
123.5	−6.71	−0.207	23.90	33.8	79.3
168.6	−6.39	−0.161	23.26	36.4	79.3
210	−6.21	−0.174	23.99	44.5	83.3
318	−9.60	−0.141	19.36	37.3	72.9

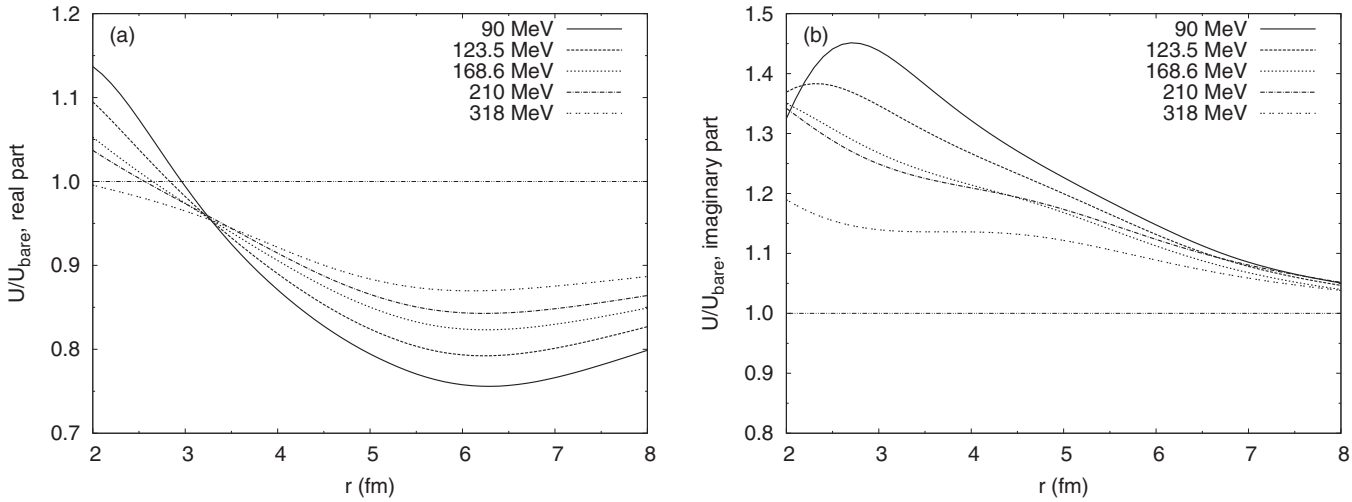

FIG. 3. Ratios between the TELP full (bare + TELP DPP) and the bare potentials for all five energies. Part (a) shows the ratio for the real part and part (b) shows the ratio for the imaginary part.

A. RESULTS OF *S*-MATRIX INVERSION

It has long been known that the real part of ^{6}Li potentials, calculated using double-folding with interactions of the M3Y type, must be reduced by around 40% to reproduce the ADs of ^{6}Li elastic scattering from nuclei [1]. This phenomenon was later attributed to the breakup coupling effects in ^{6}Li scattering [7]. We now present the local potentials that give the same ADs as the CDCC calculations by inverting the elastic-scattering *S*-matrix from those calculations. Comparison of these with the bare potentials will give a direct measure of the modification of the single-channel potential by the coupling to breakup channels.

The inverted potentials are most conveniently presented as a ratio to the bare potential. In Fig. 2 we show the ratio of $U_{\rm inverted} = U_{\rm bare} + U_{\rm DPP}$ over $U_{\rm bare}$ for both real, Fig. 2(a), and imaginary, Fig. 2(b), parts. For reference, we note that the strong absorption radius (SAR) is around 6.15 fm at 90 MeV, falling to 5.32 fm at 318 MeV. (Here we define the SAR as the classical distance of closest approach for partial wave L for which $|S_L|^2 = 0.5$.) At the SAR, the depth of the real part is reduced by about 35% at 90 MeV and by just 16 % at 318 MeV. Another view of the DPPs is given in the next section where, in Figs. 4 to 8, they are compared with those calculated using the approximate TELP procedure. We see there that the TELP yields a much smaller reduction in the real potential in the surface. In the far surface, and at the lowest energy, these results are roughly consistent with the previously found reduction factor of around 0.6 in the surface regions. But this factor rises to about 0.84 at the highest incident energy and at all energies the factor exceeds unity at smaller radii. The question then arises as to whether the change from surface repulsion to attraction further in, at about 4.2 fm for 90 MeV, is of empirical significance. We return to this question in Sec. IV.

Table II presents the changes induced by breakup in the real and imaginary volume integrals, as well as the change in the rms radius of the real term. The quantities $\Delta J_{\rm R}$ and

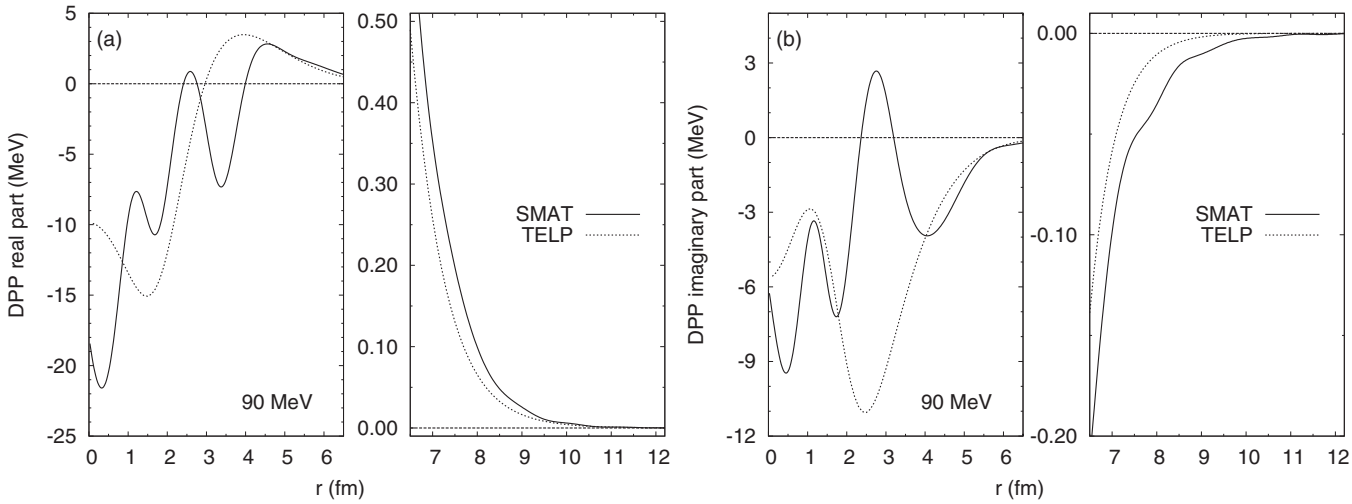

FIG. 4. Comparison of the *S*-matrix and TELP DPPs, (a) real and (b) imaginary parts, for 90 MeV.

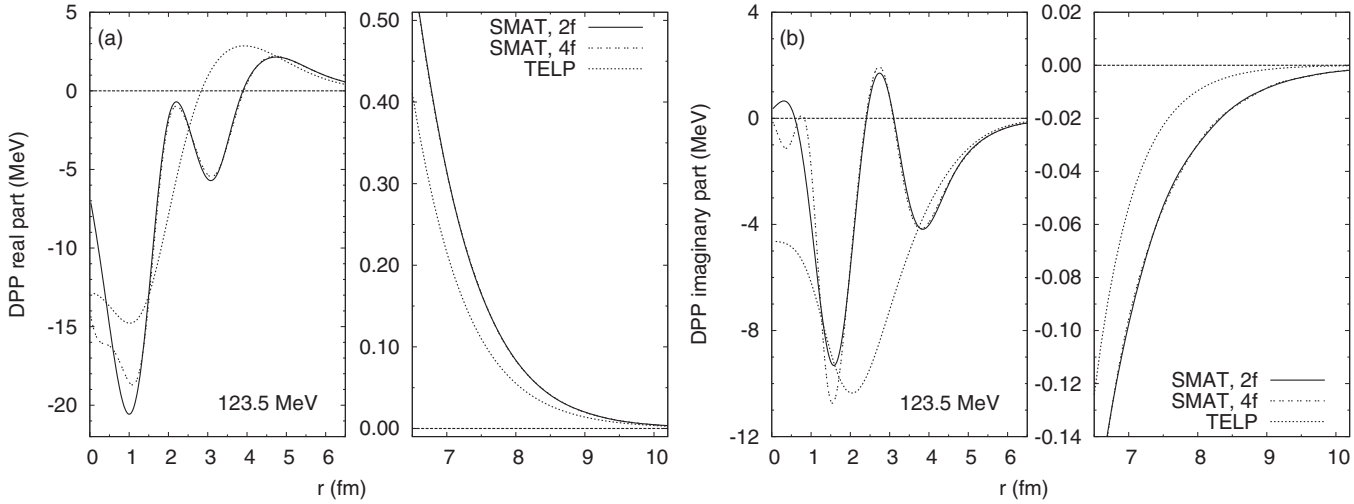

FIG. 5. Comparison of the S-matrix and TELP DPPs, (a) real and (b) imaginary parts, for 123.5 MeV. The DPPs labeled "2f" and "4f" are discussed in the text.

$\Delta J_{\rm IM}$ are just the volume integrals of the DPP itself. For example, $\Delta J_{\rm R} = J_{\rm R}$(inverted) $- J_{\rm R}$(bare). In each case $\Delta J_{\rm R}$ is small and negative; for example, at 90 MeV breakup coupling generates just a 2.71% reduction in the volume integral of the real potential (see Table I). This is much less that the 20–40% reduction of the potential in the surface that was suggested by the necessary correction of the M3Y folding model [1,2]. The small magnitude of the reduction in $J_{\rm R}$ follows from the attractive nature of the DPP within the nucleus, for example, for r less than ∼4 fm at 90 MeV, as can be seen in Fig. 2. The attractive nature of the DPPs in the nuclear interior is more evident in Figs. 4–8 discussed below. The last two columns of Table II show that, at all energies, the increase in total reaction cross section that follows the inclusion of breakup is much less than the cross section into the breakup channels. The breakup process is evidently reducing the absorption by fusion and other processes.

All S-matrix inversions yielded potentials for which the real and imaginary parts of S_L were visually indistinguishable, for all L, from the S_L from FRESCO. The only exceptions were for the highest L values ($L > 50$ for the 90 MeV case) where the very small argument of the FRESCO complex S_L exhibited fluctuations. The quality of inversion is quantified with the quantity

$$\sigma^2 = \sum_L \left| S_L^{\rm t} - S_L^{\rm i} \right|^2, \tag{1}$$

where $S_L^{\rm t}$ is the target S-matrix to be inverted and $S_L^{\rm i}$ is the S-matrix for the inverted potential. In all cases, the value of σ^2 was between 3.93×10^{-5} and 6.76×10^{-4}, this last being for the 90 MeV case. An exception is the potential labeled "2f" in Fig. 5 for which $\sigma^2 = 1.24 \times 10^{-3}$; this exhibits quite small differences from "4f," for which $\sigma^2 = 1.6 \times 10^{-4}$. These differences are primarily deep within the nuclear overlap region. The volume integrals and rms radius for 2f and 4f are very close. For the 90 MeV case, a solution with a much lower value of $\sigma^2 = 9.68 \times 10^{-5}$ was found, having more "waviness" in the surface, but with almost identical values of

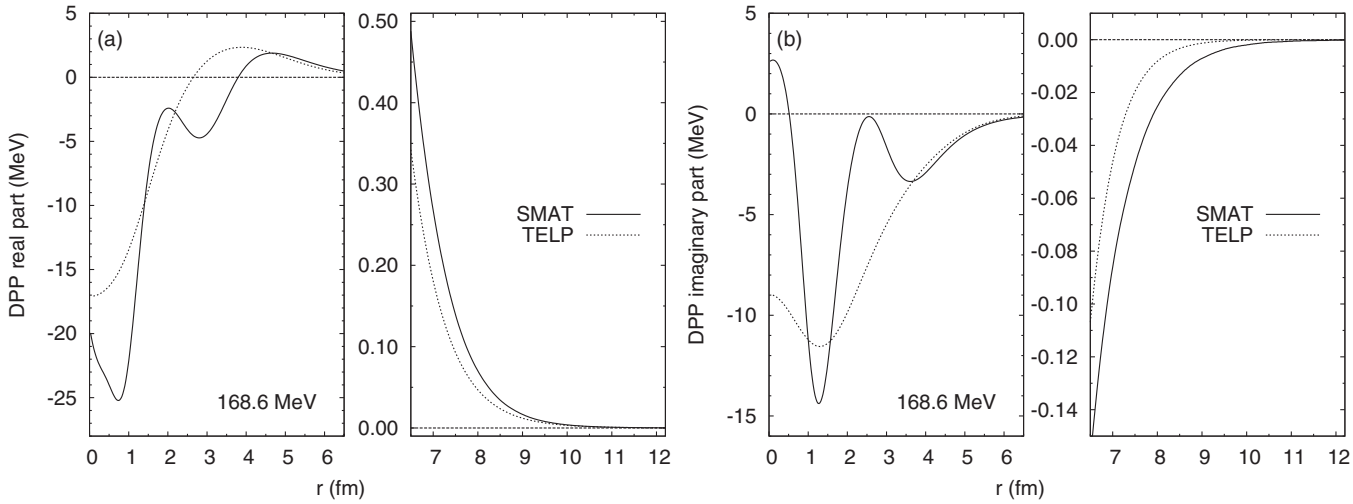

FIG. 6. Comparison of the S-matrix and TELP DPPs, (a) real and (b) imaginary parts, for 168.6 MeV.

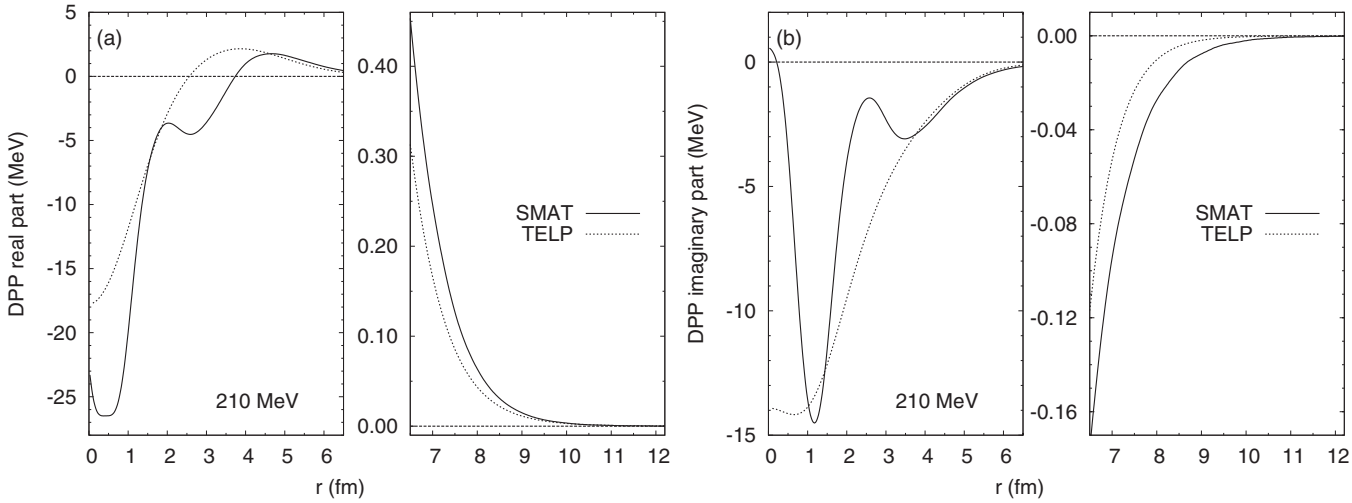

FIG. 7. Comparison of the S-matrix and TELP DPPs, (a) real and (b) imaginary parts, for 210 MeV.

the volume integrals and rms radius. Such wavy features occur with very precise inversions of S-matrix elements that have noisy features, such as the fluctuations mentioned above that occur for FRESCO S_L at high L. The values in Table II for 123.5 MeV are for the potential labeled 4f; the corresponding values for 2f are -6.93, -0.207, and 23.85. It should be remembered that $\Delta J_{\rm R}$, $\Delta R_{\rm rms}$, and $\Delta J_{\rm IM}$ are differences between large numbers so the difference in these values of $\Delta J_{\rm R}$ corresponds to a 0.26% difference in $J_{\rm R}$, the volume integral of the real potential as determined by inversion.

B. COMPARING S-MATRIX AND TELP DPPS

FRESCO makes possible the calculation of the TELP from the elastic channel wave functions of the CDCC calculations and this can be compared to the S-matrix equivalent potential. Figure 3 presents the same ratios as Fig. 2, but calculated from the TELP (the vertical scales are somewhat different). Direct comparisons between the S-matrix-equivalent DPP from the IP method and from the TELP are given in Figs. 4–8 for 90, 123.5, 168.6, 210, and 318 MeV, respectively. In all these figures, part (a) presents the real part and part (b) presents the imaginary part. We conclude the following.

(i) There are systematically non-negligible differences between the S-matrix DPP and the TELP DPP. In the external region, at all energies, both the real and the imaginary S-matrix DPPs are significantly larger in magnitude than those calculated from the TELP. There are also substantial differences in shape at smaller radii, especially at lower energies.

(ii) The real part of the DPP is internally attractive and externally repulsive for all energies.

(iii) The crossover where the real DPP changes from attractive to repulsive is at a radius, decreasing with increasing energy, where the projectile and the target nuclei overlap. We show with notch tests that the elastic-scattering cross sections are sensitive to the shapes of the optical model potentials at the crossover points. Hence, in principle, elastic-scattering measurements might be used to

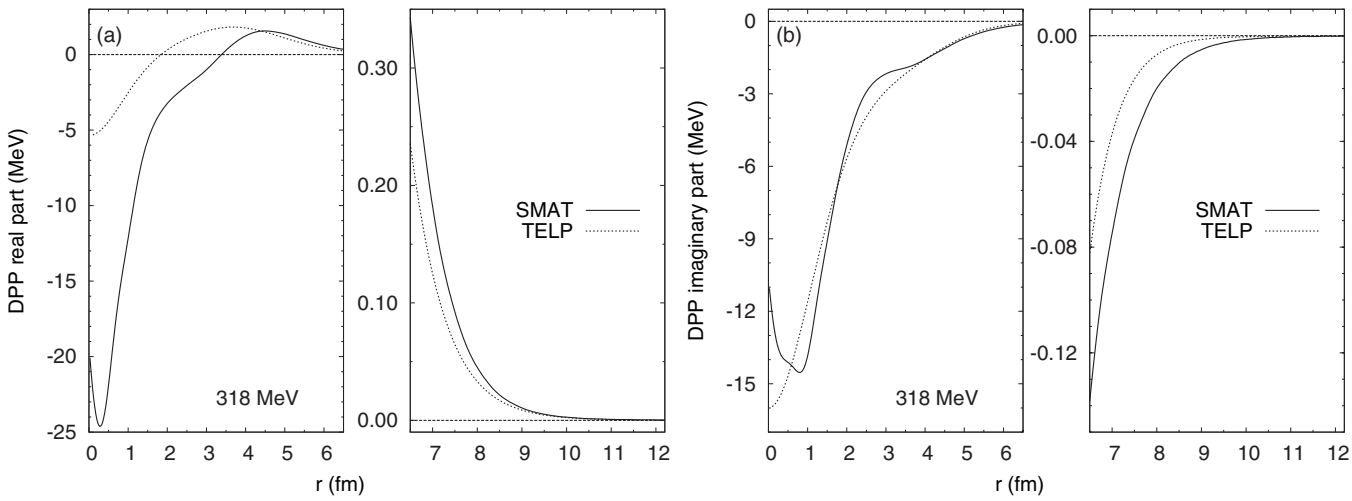

FIG. 8. Comparison of the S-matrix and TELP DPPs, (a) real and (b) imaginary parts, for 318 MeV.

determine optical model potentials at, or even within, the crossover region.

(iv) At the lower energies, the S-matrix imaginary DPP has emissive regions.

The last point alludes to the fact that, in Figs. 4 and 5 the imaginary S-matrix DPPs exhibit an interesting feature: they become emissive (generative) between 2 and 3 fm; this almost occurs at 168.6 MeV too. This is particularly noticeable at 90 MeV. The degree of emissiveness in the DPP is not such as to lead the total potential to have an emissive region, and there is no question of unitarity being broken. But there is, nevertheless, a counterintuitive behavior of $|S_L|$ that is probably related to it. This is the fact that at 90 MeV, for $12 \leqslant L \leqslant 15$, $|S_L|$ is at least equal to its no-breakup value and substantially greater for $L = 13$ and 14, as illustrated in Fig. 9, which reveals this as part of a systematic energy dependence. This particular consequence of reaction or inelastic coupling has been reported before (e.g., Refs. [9,39]) and can be predominant in lower energy reactions [45]. It appears to be related to the nonlocal and/or L-dependent nature of the underlying DPP. In Austern's account of nonlocality [46], flux is removed from one part of the interacting region and appears in another. It supports the idea that reaction channel effects cannot fully be represented in a local density folding model. We note that the apparently related emissive feature of the imaginary DPP is absent from that derived from the TELP. Finally, we note that some degree of waviness is a general feature of L-independent potentials that have the same S-matrix as explicitly L-dependent potentials (for example, see Ref. [47]).

IV. NOTCH TEST OF SENSITIVITY

To answer the question raised in Sec. III A, we study the sensitivity of elastic-scattering ADs to variations in the optical potential at different radii by applying the notch test of Wall *et al.* [48]. The notch test is applied to a single-channel calculation of scattering from the S-matrix-inverted potential at the relevant energy. In this test, the real and imaginary parts of the potential, as a function of r, are multiplied by the notch factor $f_{\rm n}(r)$:

$$f_{\rm n}(r) = 1 - s \exp\left[-\left(\frac{r - R_{\rm notch}}{a_{\rm notch}}\right)^2\right], \qquad (2)$$

with $s = 0.5$ and $a_{\rm notch} = 0.2$ fm. The notch position $R_{\rm notch}$ advances from 0 in steps of 0.1 fm. For each $R_{\rm notch}$ we calculate the corresponding χ^2 values assuming uniform uncertainties of 10% for each data point. Results of the notch tests are shown in Fig. 10 in which the χ^2 values for each energy are normalized with the χ^2 value corresponding to $R_{\rm notch} = 0$ fm (χ_0^2). One clearly sees that as the incident energy increases the elastic-scattering ADs become more sensitive to the inner part of the optical potential and the crossover points are well inside the "range of sensitivity" for each incident energy.

Visible changes in the total elastic-scattering cross sections appear for notches beyond 3.2, 3.0, 2.8, 2.5, and 2.0 fm for incident energies of 90, 123.5, 168.6, 210, and 318 MeV, respectively. Clearly the crossover points at the energies are well within these ranges, suggesting that the crossover might have observable consequences for accurate AD measurements. On the other hand, the total reaction cross sections are found to be not sensitive to the changes of the inner parts of the optical potential.

We also carried out more elaborate notch tests based on a measure of the difference between two ADs when they are compared out to some specific angle. The two ADs corresponded to scattering with and without a notch in the real potential at some specific but adjustable radius. In this way we deduced that for 90 MeV, AD data would be required out to 85° in order to be sensitive to the crossover at 4.2 fm. For 318 MeV, data out to 35° would be sensitive to the crossover at 3.5 fm. From Refs. [18–21], it would seem that suitable measurements are feasible.

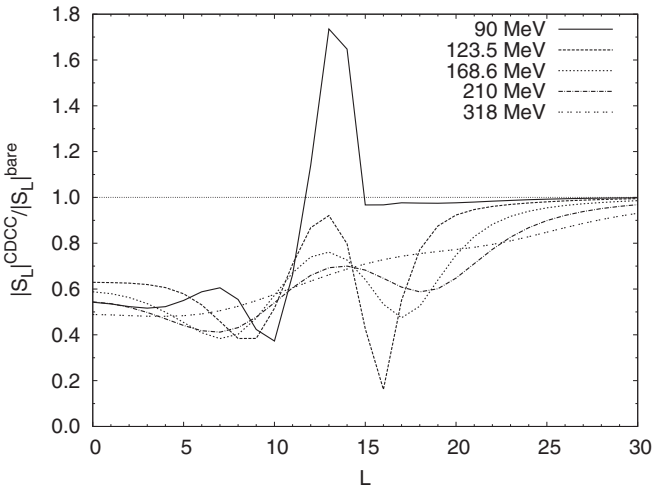

FIG. 9. For each energy and low values of orbital angular momentum quantum number L, the ratio of $|S_L|$ with breakup coupling to $|S_L|$ without breakup coupling.

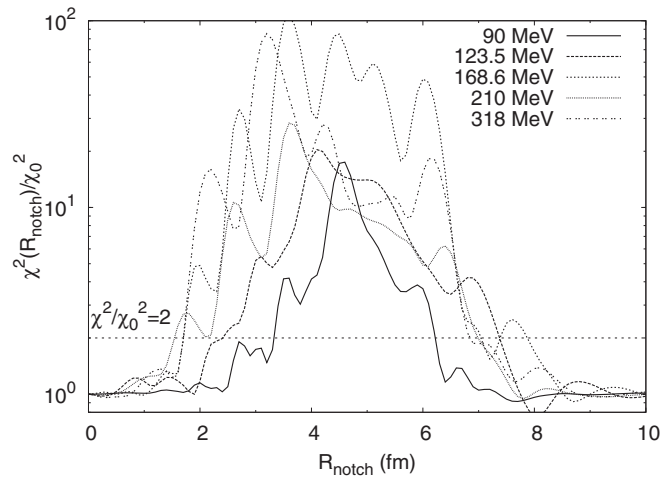

FIG. 10. For each incident energy, the ratio of the χ^2 value with notch at the indicated notch radius to the value without a notch. The notch function is specified in the text.

V. DISCUSSION OF THE RESULTS

We have shown that for a ^{6}Li nucleus incident on ^{12}C, projectile breakup generates a complex local-equivalent DPP that varies in a systematic way over the incident energy range from 90 to 318 MeV. It is the S-matrix-equivalent DPP that is more appropriate for comparing with phenomenological potentials because it corresponds to the potential that directly reproduces the scattering in a local potential model. We have compared the S-matrix DPP with that generated by the TELP procedure, which we find to be substantially different in two major respects: the magnitude is substantially less in the surface region and significant long-wavelength wavy features disappear. Among these is the emissive region that appears in the imaginary part of the S-matrix DPP at the lower energies. For the 90 MeV case, this appears to relate to an actual *increase* in $|S_L|$ around $L = 13$ induced by breakup. This may be associated with the L-dependent and nonlocal character of the underlying DPP. Concerning the difference between the TELP and exact inverted potentials, we find that, at 123.5 MeV, the AD from a single-channel calculation with the TELP + bare potential departs from the CDCC AD by 30% at 40° and by rapidly increasing amounts at greater angles. For $\theta < 30°$, the disagreement is reversed with the TELP + bare AD being some 5–30% greater than the CDCC (and S-matrix inversion) AD for angles beyond about 15°. These features can be seen in Fig. 11, together with the large effect of the breakup coupling. The AD labeled "CDCC" is, of course, also the angular distribution for the potential derived by S-matrix inversion, which is indistinguishable over this angular range.

We showed by means of notch tests that the overlap region where the real DPP changes sign might be accessible to scattering of sufficient precision and angular range.

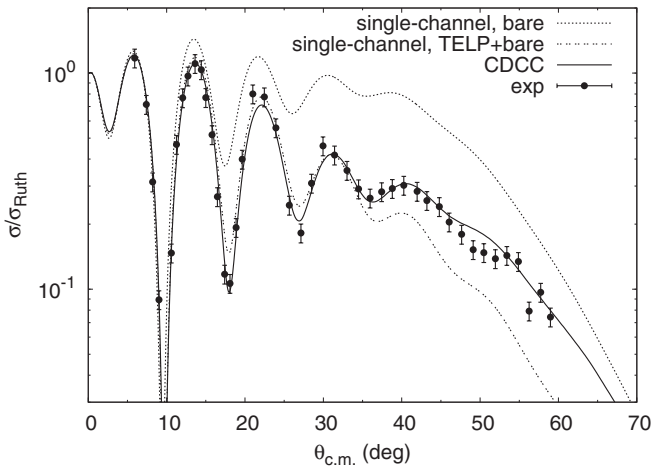

FIG. 11. The AD for 123.5 MeV ^{6}Li elastic scattering from ^{12}C. The dotted line is for the bare potential with no coupling, the solid line represents the inclusion of breakup with CDCC, and the double-dotted line is for single-channel scattering with the TELP DPP added to the bare potential. The addition of the S-matrix inverted DPP to the bare potential reproduces the solid line.

At the lowest energy, the repulsive effect in the surface is consistent with the correction factor required by the M3Y folding model. At higher energies, the surface repulsion effect becomes much less. At all energies, the volume integral of the real part of the DPP is slightly repulsive although the interior attraction appears to be a large effect. This can be attributed to the r^2 weighting of the volume integral and our results imply that breakup makes a negligible contribution to the energy dependence of the real volume integral, J_R. The combination of surface repulsion and interior attraction leads to a consistent pattern of reduction of the rms radius of the real potential. This commonly occurring feature of collective and reaction channel DPPs may be significant for attempts to measure nuclear sizes with nuclear projectiles.

A full understanding of the origin of the characteristic pattern of surface repulsion and interior attraction remains elusive, but the former might be explained as follows: In a semiclassical picture, the propagating projectile (which may be a deuteron-α pair still in close association) will have amplitudes corresponding to a range of paths through the nucleus. This range will result from, for example, the breakup excitation and the change of up to ± 2 in partial wave L value. For the higher partial waves (relevant to the DPP in the surface) these amplitudes correspond to paths that pass through a region where both the real and the imaginary potentials fall rapidly with increasing r. Those amplitudes, therefore, which are least strongly absorbed by virtue of passing through a region of lesser absorption, will also lie in a region of lesser attraction. Considering now the transition back to the elastic channel (acknowledging that second-order excitation-deexcitation is not a perfect representation of the full coupled-channel effect), those paths that correspond to least absorption will also be those along which the propagating particle (or deuteron-α pair) will receive the least additional phase, as characteristic of a weaker potential. The net effect, when the amplitudes are added to those of the unexcited propagating ^{6}Li, will be as if the ^{6}Li has propagated through a shallower potential. Hence, surface waves will experience an effective repulsive effect. It was shown long ago [10] that the L transfer appears to determine the degree of surface repulsion. In order to get some clues, we repeated the 168.6 MeV calculation with the imaginary bare potential multiplied by 0.5. With the above arguments in mind, it is not surprising that the surface repulsion of the DPP at 4.5 fm, near it maximum, was reduced by 40%. What was unexpected was that the reduction in the bare imaginary potential would lead to an increase in the absorptive DPP for $r \geqslant 4.5$ fm. Such model calculations are very easy with exact S-matrix inversion and may yield some clues, but there are many parameters to vary, making it a substantial project.

ACKNOWLEDGMENTS

DYP was supported by the National Basic Research Program of China (Grant No. 2007CB815002), the National Natural Science Foundation of China (Grants No. 11035001, No. 10775003, No. 10735010, and No. 10975006), and China Postdoctoral Science Foundation (Grant No. 20100470133).

[1] G. R. Satchler and W. G. Love, Phys. Rep. **55**, 183 (1979).
[2] G. R. Satchler, Phys. Rev. C **22**, 919 (1980).
[3] G. H. Rawitscher, Phys. Rev. C **9**, 2210 (1974).
[4] J. P. Farrell Jr., C. M. Vincent, and N. Austern, Ann. Phys. (NY) **96**, 333 (1976).
[5] M. Yahiro, N. Nakano. Y. Iseri, and M. Kamimura, Prog. Theor. Phys. **67**, 1467 (1982).
[6] N. Austern, Y. Iseri, M. Kamimura, M. Kawai, G. Rawitscher, and Y. Yahiro, Phys. Rep. **154**, 125 (1987).
[7] Y. Sakuragi, M. Yahiro, and M. Kamimura, Prog. Theor. Phys. Suppl. **89**, 136 (1986).
[8] R. S. Mackintosh and A. M. Kobos, Phys. Lett. B **116**, 95 (1982).
[9] R. S. Mackintosh and A. A. Ioannides, in *Advanced Methods in the Evaluation of Nuclear Scattering Data*, Lecture Notes in Physics Vol. 236 (Springer-Verlag, Berlin, 1985), p. 283.
[10] A. A. Ioannides and R. S. Mackintosh, Phys. Lett. B **169**, 113 (1986).
[11] T. Matsumoto, T. Egami, K. Ogata, Y. Iseri, M. Kamimura, and M. Yahiro, Phys. Rev. C **73**, 051602(R) (2006).
[12] K. Ogata, T. Matsumoto, T. Egami, Y. Iseri, M. Kamimura, and Y. Yahiro, Nucl. Phys. A **805**, 447c (2008).
[13] T. Matsumoto, K. Kato, and M. Yahiro, Phys. Rev. C **82**, 051602(R) (2010).
[14] N. C. Summers, F. M. Nunes, and I. J. Thompson, Phys. Rev. C **74**, 014606 (2006).
[15] M. Rodríguez-Gallardo, J. M. Arias, J. Gómez-Camacho, R. C. Johnson, A. M. Moro, I. J. Thompson, and J. A. Tostevin, Phys. Rev. C **77**, 064609 (2008).
[16] M. Rodríguez-Gallardo, J. M. Arias, J. Gómez-Camacho, A. M. Moro, I. J. Thompson, and J. A. Tostevin, Phys. Rev. C **80**, 051601(R) (2009).
[17] G. R. Satchler, *Direct Nuclear Reactions* (Clarendon Press, Oxford, 1983).
[18] Yu. A. Glukhov *et al.*, Yad. Fiz. **34**, 312 (1981).
[19] Y. Sakuragi, Phys. Rev. C **35**, 2161 (1987).
[20] A. Nadasen *et al.*, Phys. Rev. C **37**, 132 (1988).
[21] A. Nadasen *et al.*, Phys. Rev. C **47**, 674 (1993).
[22] Experimental Nuclear Reaction Data (EXFOR/CSISRS) [http://www.nndc.bnl.gov/exfor/exfor00.htm].
[23] K. I. Kubo and M. Hirata, Nucl. Phys. A **187**, 186 (1972).
[24] A. Pakou *et al.*, Phys. Lett. B **633**, 691 (2006).
[25] N. Keeley, K. W. Kemper, O. Momotyuk, and K. Rusek, Phys. Rev. C **77**, 057601 (2008).
[26] I. J. Thompson, Comput. Phys. Rep. **7**, 167 (1988).
[27] D. Y. Pang, Y. L. Ye, and F. R. Xu (unpublished).
[28] E. Bauge, J. P. Delaroche, and M. Girod, Phys. Rev. C **63**, 024607 (2001).
[29] D. Y. Pang, Y. L. Ye, and F. R. Xu, Phys. Rev. C **83**, 064619 (2011).
[30] M. E. Brandan and G. R. Satchler, Phys. Rep. **285**, 143 (1997).
[31] C. A. Coulter and G.R. Satchler, Nucl. Phys. A **293**, 269 (1977).
[32] G. H. Rawitscher, Nucl. Phys. A **475**, 519 (1987).
[33] B. Buck, Phys. Rev. **130**, 712 (1963).
[34] F. G. Perey, Phys. Rev. **131**, 745 (1963).
[35] N. K. Glendenning, D. L. Hendrie, and O. N. Jarvis, Phys. Lett. B **26**, 131 (1968).
[36] R. S. Mackintosh, Nucl. Phys. A **164**, 398 (1971).
[37] R. S. Mackintosh and N. Keeley, Phys. Rev. C **81**, 034612 (2010).
[38] M. A. Franey and P. J. Ellis, Phys. Rev. C **23**, 787 (1981).
[39] R. S. Mackintosh and S. G. Cooper, Nucl. Phys. A **494**, 123 (1989); Phys. Rev C **47**, 1716 (1993).
[40] M. S. Hussein, M. P. Pato, L. F. Canto, and R. Donangelo, Phys. Rev. C **23**, 926 (1981).
[41] I. J. Thompson, M. A. Nagarajan, J. S. Lilley, and M. J. Smithson, Nucl. Phys. A **505**, 84 (1989).
[42] V. I. Kukulin and R. S. Mackintosh, J. Phys. G: Nucl. Part. Phys. **30**, R1 (2004).
[43] S. G. Cooper and R. S. Mackintosh, Inverse Probl. **5**, 707 (1989).
[44] S. G. Cooper, *Notes for Imago Users*, Open University report, 1999.
[45] R. S. Mackintosh and N. Keeley, Phys. Rev. C **79**, 014611 (2009).
[46] N. Austern, Phys. Rev. **137**, B752 (1965).
[47] S. G. Cooper and R. S. Mackintosh, Z. Phys. A- Atomic Nuclei **337**, 357 (1990); S. Ait-Tahar, S. G. Cooper, and R. S. Mackintosh, Nucl. Phys. A **542**, 499 (1992).
[48] N. S. Wall, A. A. Cowley, R. C. Johnson, and A. M. Kobos, Phys. Rev. C **17**, 1315 (1978).